ELSEVIER

Journal of Nuclear Materials 241–243 (1997) 68–81

journal of nuclear materials

Helium transport and exhaust experiments in tokamaks [1]

J. Hogan [*,2]

Oak Ridge National Laboratory, Fusion Energy Division, PO Box 2008, Oak Ridge, TN 37831-6376, USA

Abstract

This is a review of recent experiments on helium transport and exhaust in tokamaks. The experiments are discussed in the light of requirements placed on alpha particle confinement for sustained ignition. The ratio of alpha particle replacement time to energy confinement time must be sufficiently small, and is used as a figure-of-merit for assessing the performance of experiments. The attainment of adequate helium removal depends most sensitively on recycling processes, pumping and boundary screening. Since no experiments exactly modeling the geometry or conditions in next step reactors have been performed, heavy emphasis is placed on identifying and understanding fundamental processes so that valid extrapolation is possible. Experiments have thus been carried out for basic regimes (L- and ELMy H-mode confinement, conventional high recycling divertor) and for improved performance conditions, both for the core (ELM-free H-mode, VH-mode, supershot, reverse shear, high β_{pol} mode) and in the edge/divertor (completely detached H-mode, detached limiter). The core helium transport database has been accumulated mainly by gas puffing experiments, where the helium source is localized at the edge. Experiments with a central helium source from helium neutral beam injection find similar behavior, for the basic confinement regimes. Work is underway to make this comparison for improved confinement regimes. Results of integrated helium transport and exhaust experiments generally show adequate helium exhaust for next step reactors, but a widely used technique for helium exhaust (argon frost pumping) has been found to have important limitations for exploration of improved divertor (gas target) regimes. There has been less activity in the study of improved core and divertor operational modes, but a database is beginning to accumulate. While the figure-of-merit parameters for helium removal are favorable for next step reactors predicated on the basic core and divertor modes, the lack of similarity with next step devices requires the use of validated models even in this case, and these have been improved considerably.

Keywords: Tokamak; Helium exhaust and control; Particle transport and confinement; Active pumping

1. Introduction

This review describes experiments carried out recently to characterize helium transport and exhaust in tokamaks. It mainly describes developments occuring since an earlier review of helium removal in tokamaks [1].

Helium ash accumulation poses a potential fundamental threat to the feasibility of magnetic confinement fusion concepts based on the D–D and D–T fusion cycles. The necessity to control the build-up of helium ash imposes constraints on core transport, edge/divertor conditions, removal efficiency and plasma-facing component and pump engineering design for fusion reactors. This situation has been recognized both in general terms, since the first fusion reactor studies [2], and in detail, starting with INTOR design studies [3].

Serious concern about helium accumulation was expressed at the outset of the modern era of large tokamak experiments. An analysis of neo-classical tokamak impurity transport predicted that "...alpha-particles are likely to stay in a reactor plasma, and hence a steady-state reactor,

* Tel.: +1-423 574 1349; fax: +1-423 576 7926; e-mail: hogan@fed.ornl.gov.

[1] This research was sponsored in part by the Office of Fusion Energy, US Department of Energy, under contract DE-AC05-96OR22464 with Lockheed Martin Energy Research.

[2] In collaboration with D.L. Hillis and M.R. Wade, Oak Ridge National Laboratory, Fusion Energy Division, PO Box 2008, Oak Ridge, TN 37831-6376, USA.

PII S0022-3115(96)00496-5

for example, will hardly be possible'' [4]. A pioneering experimental study in Doublet III inferred helium accumulation properties from electron density measurements [5]. However, it was not until the helium concentration in the core plasma was measured by charge exchange recombination spectroscopy (CERS) [6] that quantitative experiments became feasible.

INTOR design studies identified the importance of divertor helium enrichment. More efficient helium removal reduces the required on-site tritium inventory, and removal is more efficient the higher the helium enrichment at the pump. Divertor helium enrichment is the ratio $\eta \equiv f_{\mathrm{He,core}}/f_{\mathrm{He,div}}$, where $f_{\mathrm{He,core}} \equiv n_\alpha/n_e$ and $f_{\mathrm{He,div}} \equiv n_{\mathrm{He}^0}/2n_{\mathrm{H}_2}$. Modeling (and the Doublet III results mentioned earlier) suggested that a high degree of relative helium enrichment could be expected, easing INTOR pumping requirements [7]. While this subject has since been re-studied [1], the importance of close interaction between divertor models and experiments for understanding fundamental processes was thus established. Quantitative studies of the divertor enrichment question were improved with the development of the species-sensitive ('smart') Penning gauge [8]. The neutral helium concentration in the pumping region can now be determined in deuterium and tritium plasmas and compared with the core concentration measured by CERS.

With these tools in place, experimental activity on this question was greatly stimulated by the ITER Conceptual Design Activity (1988–1990). The ITER CDA performance estimates were predicated on the simultaneous attainment of enhanced energy confinement (H-mode) and adequate helium ash expulsion (through frequent ELMs) [9]. Two workshops on helium transport and exhaust characterized the status of the experimental database at that time [10,11]. Only a limited database of results in limiter tokamaks and in L-mode conditions was available [12–16]. Thus, doubts remained about the fusion relevance of H-mode at the outset of the ITER Engineering Design Activity (EDA). It was thought that the short term benefits of H-mode, although yielding a greater fusion power, would be deleterious in a longer pulse because of the concomitant higher level of alpha particle ash production and the subsequent ash poisoning [17]. Therefore a high priority was given to the characterization of helium transport and exhaust in ELMy H-mode. As a result of the ITER emphasis a number of experimental campaigns on this topic were carried out on major tokamaks.

The demonstration of adequate exhaust in ELMy H-mode has now been accomplished. Core helium confinement has been studied in DIII-D [18–24], TFTR [25–28], JET [29–31] and JT-60 and JT-60U [32–34]. Helium exhaust has been successfully demonstrated in DIII-D [23,24,35], JT-60U [34], ASDEX-Upgrade [36,37], Tore Supra [38], TdeV [39], TEXTOR [40] and JET [29] for both divertor and limiter configurations. The 'CDA question', whether simultaneous attainment of adequate helium exhaust and improved confinement in a conventional high recycling divertor is possible, has been answered in the affirmative.

During this same period, though, more promising confinement regimes have been identified and new issues have arisen. ELM-free H-mode, VH-mode and Enhanced Reverse Shear (or Negative Central Shear) configurations have further increased both confinement quality and beta values. The ITER EDA has stimulated experimental attempts to improve divertor operation (reducing the divertor plate heat flux) by operation in partially or fully detached conditions with substantial edge radiation cooling.

The present status of the experimental database was discussed recently at a 3rd International Workshop on Helium Transport and Exhaust [41]. This survey showed that to date, while there is an emerging database in these new core and divertor operational regimes, there has been little systematic characterization of helium transport and exhaust. Hence, this paper addresses the status of the database in the light of new developments and thus examines (Section 2) the requirements for reactors and (Section 3) the associated basic processes involved in helium removal. The status of the present database is described in Section 4.

2. Reactor requirements for efficient helium removal

The reliability of present experiments for predicting future reactor ash accumulation depends on the similarity between experimental parameters and assumed reactor conditions, with respect to the fundamental processes which yield efficient helium removal. Reactor performance requirements directly impose limits on ash accumulation. Since experimental results are often expressed either in terms of reactor performance figures-of-merit or in terms of empirical characteristic times for basic helium transport processes, these topics are discussed first.

2.1. Helium particle balance

The helium exhaust problem is best characterized by tracing the pathway of the helium in the system. Fusion-produced helium is confined in the core (separatrix-bounded) plasma for a characteristic 'first pass' time, denoted τ_α^1, which includes both the slowing down of the fusion-produced α particle to thermal energy, and the time required by the thermalized α to diffuse to the separatrix. Possible kinetic effects, for example ripple loss or Toroidal Alfven Eigenmode (TAE) instabilities, could play a role here. After τ_α^1, the α particle enters the scrape-off layer (SOL). The SOL transport processes (such as thermal and friction forces, parallel and radial diffusion) enter. From the SOL it will probably reach the divertor plate, to be reflected, absorbed or re-emitted after neutralization. This recycled helium can be ionized in the SOL and return to the core as a (relatively) cold ion, return to the core as a fast reflected neutral, repeat the divertor plate experience,

or enter the pumping duct. From the duct it can be exhausted or return to the scrape-off layer, to repeat the SOL and divertor plate experiences. Some fraction of the first pass core efflux returns to the core, as an additional source of helium in the core due to recycling from the exterior. Since this returning source is edge-localized, the confinement time for recycled particles is described by a separate (and smaller) characteristic lifetime, τ_α^2.

From elementary particle balance the global replacement time for alpha particles is $\tau_\alpha^* = \tau_\alpha^1 + \tau_\alpha^2 R_{He}/(1 - R_{He})$. where R_{He} is the global core recycling coefficient. The value of R_{He} is determined by the helium exhaust efficiency (ε, typically $\ll 1$), and by the boundary screening parameter, γ, (also $\ll 1$) for unpumped helium: $R_{He} = \gamma/(\varepsilon + \gamma)$ [42]. The first pass of helium exhaust depends mostly on intrinsic core confinement (τ_α^1) and after that the edge, divertor, pumping and SOL screening properties (γ, ε, τ_α^2) determine the eventual level of accumulation. The stationary helium concentration in large machines is determined mainly by γ, ε, and τ_α^2 [1], so the helium removal problem is sensitive to the details of the divertor pumping geometry.

Although direct measurements of τ_α^1, τ_α^2, γ and ε would be desirable, some experimental parameters characterizing helium transport and removal are more easily observable. The helium particle balance in pumped divertor experiments is often discussed in terms of a 'multi-reservoir' model describing evolution of the total number of particles in the core, divertor/SOL and pump (N_{core}, N_{div}, N_{pump}) in terms of characteristic decay constants τ_{core}, τ_{div} and τ_{pump} [37,43,44]. For example,

$$\begin{aligned}
\frac{dN_{core}}{dt} &= \Sigma_{D-T} - \frac{N_{core}}{\tau_{core}} + \frac{N_{div}}{\tau_{div}} \\
\frac{dN_{div}}{dt} &= -\frac{N_{div}}{\tau_{div}} + \frac{N_{core}}{\tau_{core}} - (1 - \varepsilon_{cond})\Phi_{baffle} \\
\frac{dN_{pump}}{dt} &= (1 - \varepsilon_{cond})\Phi_{baffle} - \frac{N_{pump}}{\tau_{pump}}.
\end{aligned} \tag{1}$$

This illustrates the overall particle balance, but the observed decay for N_{core}, N_{div} and N_{pump} each combine several fundamental processes. The change in core boundary conditions due to edge effects influences evolution on the τ_{core} timescale. Absorption, reflection, ionization and pump conductance processes near the divertor plate are combined in the τ_{div} timescale. The flux of helium into the pump plenum (Φ_{baffle}), the back-conductance (ε_{cond}) of unpumped helium into the SOL, and the helium pumping rate are combined in the decay seen on the τ_{pump} timescale. 'Profile relaxation' experiments determine τ_{plasma}, using a gas puff to determine the 'e-folding' time for relaxation to a steady state spatial distribution ($\tau_{1/e,He}$). This definition also combines several more fundamental processes. For example, τ_{plasma} depends on the timescale for evolution of the edge boundary conditions for core transport, and these change on the τ_{div} and τ_{pump} time scales.

2.2. Reactor criteria

2.2.1. General criteria

The requirements for a sustained burn have been derived by several authors (as described in Ref. [1]). The necessary (Wolf–Reiter) criterion states that there is a maximum ratio of the alpha particle replacement time to gross energy confinement time τ_α^*/τ_E ($\equiv \rho_{WR}$) which can be tolerated. This maximum value depends on other conditions, such as the intrinsic impurity level. With, e.g., 2% Be content, $\rho_{WR} < 10$ is needed to maintain the thermonuclear burn. If radiation losses are excluded from τ_E, the value of ρ_{WR} must be substantially smaller than 10 (Wolf, in Ref. [41]). Since the addition of efficiently radiating impurities is seen as a promising way to reduce the divertor plate heat flux, the relation between ρ_{WR} and the allowable 'fatal fraction' of other impurities is important. As shown in Fig. 1, the permissible ρ_{WR} drops very sharply for candidate radiators as their concentration (f_{imp}) rises, when the ignition parameter is fixed at $n_e\tau_E T = 10^{22}$ keV s m^{-3} [45]. Since the maximum radiated power increases with f_{imp}, divertor experiments must establish the trade-off between PWR and f_{imp}. The same requirements also apply for helical systems [46], but this subject is just now beginning to be explored experimentally.

Reactor criteria thus impose overall constraints on the transport due to core (τ_α^1) and edge recyled (τ_α^2) helium, and on the re-penetration and exhaust characteristics of the device, $R_{He}(\varepsilon, \gamma)$. Experimental study of helium transport and exhaust is thus partially separable into the study of core confinement properties and the study of re-penetration and exhaust processes.

2.2.2. Specific criteria (ITER-EDA)

While helium transport is an interesting research area for existing tokamaks, it is a sine qua non for proposed long pulse ignited tokamaks. Thus the specific research needs for the ITER design play an important role in

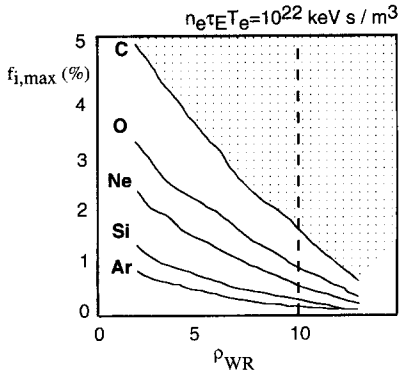

Fig. 1. Maximum tolerable impurity fraction f_{imp} versus ρ_{WR} for fixed confinement ($n_e\tau_E T = 10^{22}$ keV s m^{-3}) for candidate radiator impurities.

determining future experiments in this area. The ITER divertor design requires, simultaneously, significant divertor heat flux reduction, core Z_{eff} below 1.6, strong flow recirculation and pumping, high quality baffling, low target plate T_e, and divertor plate survivability for ELM burn-through and disruptions [47,48]. Impurity retention in the divertor is crucial to optimizing radiative efficiency [49]. While the geometry needed to support detachment is presently under study, the ITER design will be able to accommodate the wide gas box with transparent wall, vertical target and deep slot designs (Janeschitz in Ref. [41]).

These requirements also necessarily specify the relevant environment for helium transport and exhaust experiments. The design assumes that $\rho_{WR} \leq 10$, and that the helium enrichment factor, $\eta > 0.2$. The latter constraint implies a minimum $\sim 2\%$ helium concentration in the divertor plasma since $f_{He,core} \leq 12\%$ is also a design goal. Given the range of expected D–T baffle pressures (0.5–10 Pa), this requires a maximum helium pumping speed of ~ 80 m^3/s. The pumping speed provided for exhaust is 200 m^3/s. So, if $\eta < 0.2$ is found in current experiments this would suggest a reinvestigation of the ITER design assumptions.

3. Fundamental processes in helium removal

While empirical decay constants are useful to categorize the phenomena, it is recognized that the understanding needed for reliable design of future systems also requires insight into details of the more complex core transport and edge/divertor fundamental processes. Since the problem is separable into core confinement properties and the study of re-penetration and exhaust processes, the core processes are described in Section 3.1, the edge/divertor processes in Section 3.2 and the existing experimental environment for these studies (configurations and pumping) is described in Section 3.3.

3.1. Core transport: $\tau_{plasma}(\tau_\alpha^1, \tau_\alpha^2)$

In order to extrapolate the results of present core transport experiments, a description of the underlying transport coefficients is needed. The analysis of core thermal helium transport was first made with the Multiple Impurity Species Transport (MIST) code [50]. The evolution of the flux-surface averaged alpha density, n_α, in the fully ionized core plasma is described in terms of the flux-surface averaged radial diffusion equation

$$\frac{\partial n_\alpha}{\partial t} + \frac{1}{r}\frac{\partial}{\partial r}(r\Gamma_\alpha) = S_\alpha$$

$$\text{with } \Gamma_\alpha = -D_A(r)\frac{\partial n_\alpha}{\partial r} + V_A(r)n_\alpha, \qquad (2)$$

where Γ_α is alpha radial flux density, r is the normalized radius (in toroidal flux coordinates), S_α is the source, and D_A and V_A are the anomalous diffusivity and radial convective velocity. Appropriate boundary conditions determined by divertor/SOL conditions are also specified. The convective velocity V_A is parametrized in MIST as

$$v_A(r) = c_v D_A \frac{\partial(\ln n_e)}{\partial r}. \qquad (3)$$

The one-dimensional evolution $n_\alpha(r,t)$ is reduced to the specification of dependence on two radial functions $D_A(r)$ and $V_A(r)$ by Eq. (2). Since the n_e profile is measured, Eq. (3) allows a further reduction to a single radial profile (D_A) and one coefficient, c_v. The motivation is that in the fully ionized, source-free core region the stationarity condition $\Gamma_\alpha = 0$ results in a profile $n_\alpha(r) = An_e(r)^{c_v}$ where c_v measures the degree of preferential helium accumulation with respect to the n_e profile. ($c_v = 1$ means the n_e and n_α profiles have the same shape.) For the special case of a parabolic n_e profile Eq. (2) becomes $V_A = -2D_A c_v r/a^2$. Experimental results for impurity transport are often quoted using the approximate parametrization, but this is not valid for the broad (or even inverted) n_e profiles measured in enhanced confinement regimes in divertor tokamaks. The radial model describes diffusive processes, and while some effects of faster MHD time-scale phenomena (sawteeth and ELMs) enter indirectly through their modification of the n_e profile, the alpha-specific MHD effects must be determined separately.

An important simplification can be made in the core plasma region if (i) the helium is fully ionized and (ii) $S_\alpha = 0$. In that case the right hand side of Eq. (2) vanishes and the flux $\Gamma_\alpha(r, t)$ may be determined directly from measurement of $n_\alpha(r, t)$, by CERS for example. This allows a direct determination of D_A and V_A for the source-free region. This approach has been used for TFTR [27], on DIII-D [23] and for JET [29]. Fig. 2 shows the results of such an analysis for TFTR: a comparison for L-mode and Supershot conditions of the inferred radial profiles of the helium and ion thermal diffusivity from the source-free analysis and from MIST (Synakowski in Ref. [10]). Values for D_A and V_A obtained by the direct and MIST modeling techniques overlap in the region of common validity. Analysis of the measured fluxes and gradients requires careful treatment in the applicable regime for the source-free assumption. In JET, for example, typically, the region in which normalized radius $\rho > 0.8$ has sources, while the inner region is characterized by complex CERS spectra and gradients which are near zero (von Hellermann in Ref. [41]).

Where the source-free assumption is not valid, modeling with time dependent impurity transport codes, such as MIST, using measured background plasma profiles, is used to infer D_A and V_A from fits to CERS radial profiles. Since some of the same difficulties are encountered (near zero

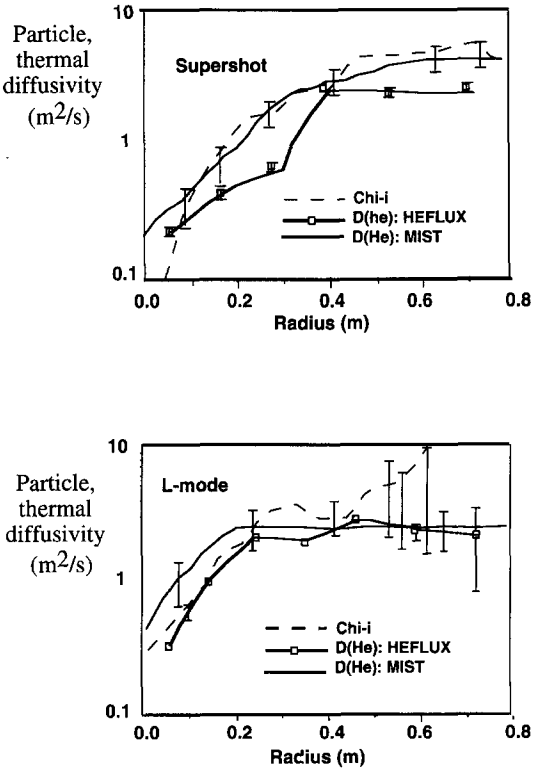

Fig. 2. Comparison of radial particle diffusivity coefficients for helium and thermal ion diffusivity in TFTR, using both the direct analysis and MIST transport code methods, for L-mode and supershot conditions.

gradients in steady-state conditions) MIST transport coefficients are inferred from the initial transient after the gas puff is injected [20].

The work required to provide an adequate atomic physics database is another fundamental aspect of this effort. The Atomic Data and Analysis Structure (ADAS) database provides the data needed for CERS [51]. Even though great progress has been made in this area, there remain some problems. For example, the neutral beam geometry on JET produces a strong neutral beam 'plume' effect which can distort the CERS measurement. Very detailed work is required to extract results, but helium still cannot be used as a reliable indicator of plasma temperature and density.

3.2. Divertor / edge / pump processes τ_{div}, $\tau_{pump}(\gamma, \varepsilon)$

3.2.1. Divertor / edge processes: τ_{Div}

A detailed two-dimensional conceptual model, based on moments of the kinetic equations, has been developed for transport processes in conventional high-recycling divertor, using transport codes such as b2 [52] and DIVIMP [53,54] and the UEDA code [55]. This construct has helped to guide experimental studies. Some of the important processes can be identified just from the parallel force balance for alphas, which is described by

$$\frac{\mathrm{d}(n_\alpha T_\mathrm{i})}{\mathrm{d}l} - 2eE_\parallel n_\alpha = U_{\alpha,\mathrm{p}}(V_\alpha - V_\mathrm{p}) + n_\alpha\left(\frac{4C_\mathrm{e}}{Z_\mathrm{i}}\frac{\partial T_\mathrm{e}}{\partial l} + C_\mathrm{i}\frac{\partial T_\mathrm{i}}{\partial l}\right), \quad (4)$$

where l is the coordinate along the magnetic field away from the divertor plate, $C_{e,i}$ are the electron, ion thermal force coefficients, $V_{\alpha,p}$ are the alpha and background flow velocities which determine the collisional friction force [56,57]. According to this model, the thermal force disperses recycled helium ions away from the divertor and allows better re-penetration to the core plasma, while the retarding friction force with the background flow toward the divertor plate increases retention in the divertor. Direct experimental identification of these forces is difficult because, for example, the intense gas puffing which is often used to increase the hydrogenic flow toward the divertor, and thus increase the retarding frictional force, also reduces T_i and thus reduces the thermal force as well.

If friction with the background plasma is high enough, then the radial variation also becomes important. The helium flux is directed radially away from the local D–T density maximum at the strike point, and so the helium density is shifted outward of the separatrix. For example, since this effect directs the helium flux toward the pump duct entrance, calculations for the ITER CDA design produced a favorable prediction for helium exhaust [58]. However, these calculations did not self-consistently couple the neutral and ion populations. Implicitly coupled models for neutral and ion transport have since been developed [59], and are now being compared with experimental results [60,61] and applied to the ITER EDA design [62,63]. The enhanced divertor performance in the ITER EDA design (Section 2.2.2) requires high neutral density and pressure in the divertor. Atomic physics processes related to ion–neutral and neutral–neutral interactions are involved which have hitherto been neglected. These processes are also now incorporated in the models [64–66].

3.2.2. Pumping processes: τ_{pump}

The fact that helium is a noble gas implies that it will recycle with a near unity coefficient from plasma-facing surfaces. However, significant absorption of helium by beryllium has been measured on JET [67], helium absorption by boronized surfaces is an integral part of the Solid Target Boronization (STB) helium exhaust technique used on JT-60 [34] and helium absorption is found on well-conditioned graphite limiters in TFTR [68].

Divertor exhaust experiments on DIII-D and JET use the technique of covering the cryopump with a layer of argon frost. Helium is trapped in the argon layer only transiently. However, the rate of helium removal with this

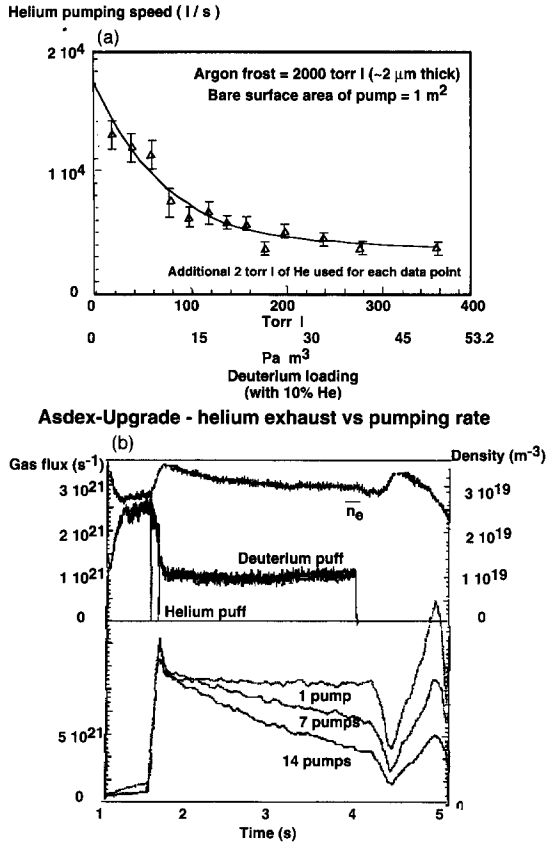

Fig. 3. Pumping systems comparison. (a) Variation of helium pumping speed in the DIII-D cryopumping system versus D_2 flux. (b) Measured helium density decay in Asdex Upgrade ohmic conditions as the number of active pumps is increased.

technique depends sensitively on the prior history of loading of the argon layer by D_2. Fig. 3a shows the measured variation of pumping speed for an argon frost layer on the DIII-D cryo-pump, as a function of the accumulated D_2 on this pump [69]. Approximately 100 Torr l (~ 13 Pa m^3) of D_2 is sufficient to reduce the active helium pumping speed by 2/3. This is a serious drawback to use of this technique in detached plasma studies, where D_2 gas puff rates in excess of 100 Torr l s^{-1} (13 Pa m^3 s^{-1}) are often used.

In contrast, helium exhaust experiments carried out with turbomolecular pumps can continuously exhaust helium even with high fluences of D_2 and for steady conditions [70]. As a bonus, they allow an extrapolation in pumping speed, since the number of active pumps can be varied. This additional control has been exploited in a recent Asdex Upgrade experiment which has succeeded to decouple the external gas flow from the friction force using turbomechanical pumping [71]. Fig. 3b shows an example of the capability to vary the pumping speed with turbomolecular pumping in ASDEX-Upgrade. The helium decay rate (as measured by helium recycling at the inner wall) increases as the number of active pumps is increased (Bosch in Ref. [41]).

3.3. Divertor and pumping configurations

Helium transport and exhaust experiments have been carried out in a number of different types of plasma and divertor configurations, so that the accumulation of a uniform database which could be directly empirically extrapolated for use in the design of future machines is difficult. Table 1 (prepared by D. Campbell, JET) presents a survey of the plasma and pump types, and helium

Table 1
Survey of existing and planned upgraded capabilities for helium transport and exhaust experiments (prepared by D. Campbell, JET)

Helium pumping capabilities						
Tokamak	Plasma type	Pump [a]	Speed (m^3 s^{-1})	Plasma volume (m^3)	Pump geometry [b]	Helium pumping [c]
JET (MkI/MkII [d])	divertor	CY	180	80	O/P	Ar
JT-60U (modif.) [d]	divertor	CY	35–72	50–80	I/I + O	STB/Ar
DIII-D	divertor	CY	18	21	O/P	Ar
Asdex-U (Lyra) [d]	divertor	TM/CY	14/100	13	O(P)	TM(Ar)
JFT-2M	divertor	CY	1.9	2.5	O	Ar
TdeV	divertor	CY	6/4	1	O	AC
C-Mod [d]	divertor	CY	10	0.9	O	Ar
TRTR	limiter	wall	(varies)	60	limiter	wall
Tore Supra	lim/erg. div.	Ti	25–40	25	limiter	wall
TS Continu [d]	lim/erg. div.	CM	12–60	25	limiter	CM
TEXTOR	lim/erg/ div.[4]	TM	5.6	7	limiter	TM

[a] Pump: TM: turbomolecular, CY: cryopump, CM: cryo-mechanical, Ti: titanium getter.
[b] Pump geometry: I: inner leg, O: outer leg, P: private flux.
[c] Helium pumping: TM: turbomolecular, Ar: argon frost, CM: cryo-mechanical, STB: solid target boronization, AC: activated charcoal.
[d] Status: indicates not yet operational capability.

pumping types for experiments now operating, or for upgrades which are planned or proposed.

4. Status of experiments

The attainment of satisfactory helium removal depends both on adequate core transport, involving τ_α^1, τ_α^2, and on effective helium removal, which involves $R_{He}(\gamma, \varepsilon)$. Work in this area has mainly concentrated on characterization of basic confinement modes (L-mode and ELMy H-mode) combined with basic edge and divertor modes (limiter and conventional high recycling conditions). However, a database is also beginning to form on aspects of enhanced regimes as well, both for enhanced core confinement modes and for enhanced divertor performance. The experimental results are discussed in terms of core transport (Section 4.1), divertor/edge processes (Section 4.2) and then the results of integrated helium removal experiments (Section 4.3).

4.1. Core helium transport: $\tau_{plasma}(\tau_\alpha^1, \tau_\alpha^2)$

Core helium transport work has, for the first time, involved studies of D–T fusion produced alphas in TFTR, and further results are expected from JET in the near future (Section 4.1.1). Kinetic theory and modeling aspects of alpha particle transport, with a special emphasis on TFTR D–T experiments, have been discussed in a dedicated issue of Nuclear Fusion [72]. The transport of non-nuclear alphas has mainly been measured in experiments in which a short gas puff of helium is injected, and the subsequent evolution is observed. This technique has allowed exploration of the dependence of alpha transport in both basic and enhanced confinement regimes (Section 4.1.2). Several comparisons of gas puffing (which emphasizes τ_α^2) with helium neutral beam injection (providing a central α source) have been carried out (Section 4.1.3).

4.1.1. Fusion-produced alphas

TFTR D–T experiments and analysis have covered the life cycle of a particle ash, from thermonuclear production to pumping by the TFTR bumper limiter (Synakowski in Ref. [41]).

The energy spectrum of confined, slowing alphas near the 3.52 MeV birth energy has been measured with the help of boron pellet injection. With pellets injected 0.2 s after a 1 s neutral beam pulse a classical slowing spectrum down to 1 MeV is found, while with pellets injected 20 ms after a shorter neutral beam pulse one finds the expected localization around the birth energy. Similar measurements show that a sawtooth event can lead to an outward radial redistribution of energetic α-particles. The fast α loss fraction is found to be constant with increasing power, but reduced with increasing I_p. The alpha behavior at intermediate energy (from 0.1–0.7 MeV) has been studied with the 'α-CHERS' diagnostic [73]. The α energy spectrum for radii $\rho = 0.05$–0.6 was compared with the f_α provided by the TRANSP analysis code [74]. The α source, collisional slowing and perpendicular diffusion using an a diffusivity $D_\alpha = 0.03$ m^2/s is consistent with the data. Ripple loss of alphas in TFTR has been analyzed with TRANSP and with the ORBIT fast ion code, showing that TFTR ripple losses could reduce the helium ash profile by 11% for standard discharges ($R = 2.5$ m) (Redi in Ref. [41]).

The thermal alpha transport coefficients (and pinch velocity) have been found to be consistent with those deduced from the results of gas puffing experiments, and the profile shape appears to be dominated by transport, and not by the localized D–T source near the axis [25].

4.1.2. Thermal α transport: Gas puff experiments

The bulk of the present database for helium transport has been accumulated with short helium gas puffs followed by observation of the subsequent evolution. Fig. 4

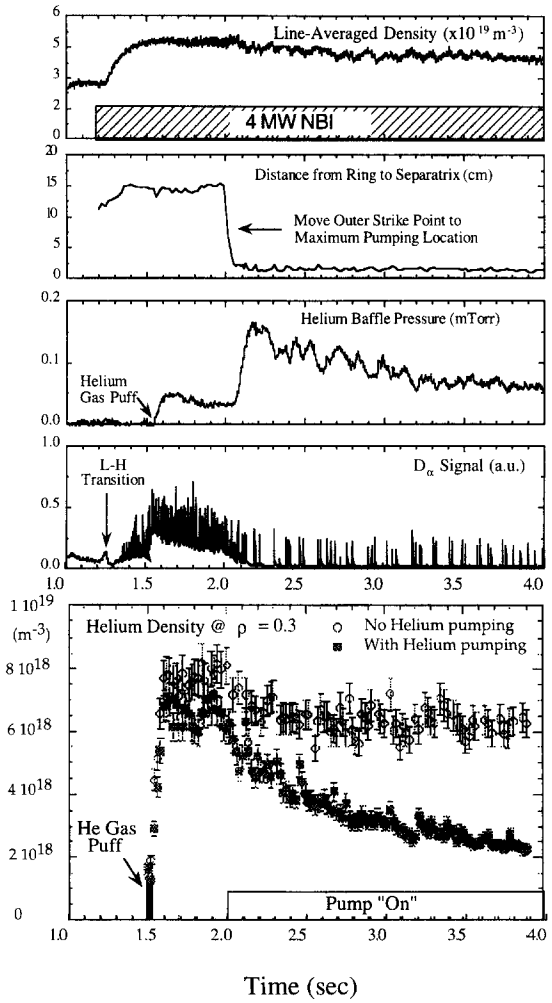

Fig. 4. Helium gas puff exhaust scenario in DIII-D.

shows the scenario for such an experiment on DIII-D. The H-mode is established with the onset of neutral beam heating, while the plasma is positioned away from the baffle entrance, so there is little pumping. The helium is introduced at the midplane, and arrives in the discharge center in ~ 100 ms. Subsequent to that, without pumping, the helium reaches a steady-state profile. Gas puff experiments combine measurements of τ_α^2 and (after the injected helium reaches the center) τ_α^1. The experiments to date have been carried out for both basic (L-mode, ELMy H-mode) and enhanced confinement modes.

4.1.2.1. L-mode. L-mode helium confinement was studied on DIII-D [75]. MIST code modeling showed similar values for D_A (~ 1 m^2/s) and c_v (1.0) as for earlier L-mode confinement measurements on TEXTOR [14] and JT-60 [76]. The first L-mode helium transport experiments in TEXTOR, made with a 3-channel CERS system [14], have been revisited in TEXTOR-94 with a 12 channel system. The more detailed profile measurement shows that the helium profile shape remains unchanged during decay. The value of ρ_{WR} is found to be ~ 12 (L-mode), somewhat higher than values previously observed in TEXTOR. The recent results were obtained under conditions in which alignment errors may result in less efficient pumping, and time dependent MIST modeling is consistent with such an explanation (Post-Zwicker in Ref. [41]).

4.1.2.2. ELMy H-mode. Experiments establishing scaling of helium transport in ELMy H-mode have been performed in DIII-D [20]. H-mode parameter scaling, based on a multiplier times ITER (89P) L-mode scaling [9], would predict $\tau_{He} \sim I_p^{0.85} n_e^{0.1} P_{in}^{-0.5}$ for a given device and configuration. For fixed injected power, the plasma current was varied from 0.6–1.6 MA. The scaling dependence observed was $D_A(\text{core}) \sim I_p^{-0.71}$ and $D_A(\text{edge}) \sim I_p^{-1.41}$, with $c_v = 1$, consistent with the range expected from H-mode scaling ($\tau \sim I_p^{0.85}$). (The $c_v = 1$ assumption is based on the observed similarity of n_e and n_α profiles in steady state.) The D_A (edge) scaling in ELMy H-mode is sensitive to the frequency and amplitude of ELMs, since helium is observed to be directly expelled from the edge plasma ($\rho > 0.8$) by ELMs [19]. Determination of the scaling dependence on neutral beam power at fixed plasma current is complicated by the fact that the ELM frequency changes with P_{NB}. Thus, as P_{NB} increases from 4 to 12.5 MW with $I_p = 1.6$ MA, the ELM frequency increases from 0 (ELM-free H-mode) to 120 Hz. τ_E decreases by a factor 3, (H-mode scaling would predict a factor 1.77 decrease), while the value of D_{He}/χ_E increased from 0.3 to 1.3. (χ_E is determined from the ONETWO analysis code). Thus, ELM effects preferentially remove particles from the edge without seriously degrading energy confinement.

The correlation between profile relaxation time (Section 2.1) and the energy confinement time has been measured for ELMy H-mode conditions on JET. The profile relaxation time for helium and neon is found to be comparable with τ_E for both H- and L-mode The n_α profile, in contrast with hollow profiles observed for beryllium, neon and carbon, assumes a shape similar to the n_e profile [29].

4.1.2.3. Enhanced confinement modes: ELM-free H-mode, VH-mode, supershot. A survey of the helium transport in enhanced confinement regimes has been possible in DIII-D because of its configurational flexibility. Fig. 5a compares the steady-state helium and electron density spatial profiles for L-mode, ELMy H-mode, ELM-free H-mode and VH-mode in DIII-D [21]. These profiles are measured 1 s after a He gas puff, so there is adequate time for relaxation to steady state. The remarkable profile consistency between α particle and n_e profiles is evident ($c_v = 1$). Transport analysis using the direct analysis method has compared D_{He} and χ_E spatial profiles for these modes, and the results are shown in Fig. 5b [21]. A systematic decrease in helium particle diffusivity is seen to accompany enhanced thermal confinement.

Comparison of helium transport in L-mode and supershot conditions in TFTR shows a more peaked helium profile in the supershot case, consistent with a stronger-than neo-classical inward convective velocity. While this in itself would not be favorable for supershot scaling to reactor conditions, it is also found that particle diffusivity and ion thermal conductivity scale together, which is a favorable result [26].

4.1.3. Helium beam injection experiments and beam / gas puff comparisons

Experiments using helium neutral beam injection to provide a central helium source to simulate D–T ash production have been made on several tokamaks. Quantitative transport studies are based on the estimation of the central helium source from the beam. The presence of long-lived helium metastables can possibly enhance the stopping cross section and reduce beam penetration to the plasma center. Measurements on JT-60 have shown that, with a 20% metastable fraction in the incident helium beam, the stopping cross section was increased by less than 10% [77].

Helium neutral beam injection experiments on JET show that the helium profile relaxes to the equilibrium shape quickly after a neutral beam pulse, so that pumping and recycling determine the profile shape rather than core transport [31]. However, somewhat disappointingly, diffusivity values $D = 0.5$ m^2 s^{-1} or 20 m^2 s^{-1} give the same final profiles with helium neutral beam injection, even with given source and measured profiles. This is a result of the fact that the fluxes are close to zero (von Hellermann in Ref. [41]).

On JT-60U, helium fueling by neutral beam injection and by gas puffing were compared. The helium content in both the core and the divertor increased linearly with time in the beam case, each reaching a saturation level of 10%,

while the enrichment of the helium density (core/divertor) remained constant (~ 1.0). For helium gas puffing with ELMy H-mode the helium content reached a saturation level of 4% after a 1 s gas puff. For a helium gas puff during L-mode, the concentration required only a 0.5 s helium gas puff to reach the 5% level. There is a 4 × larger

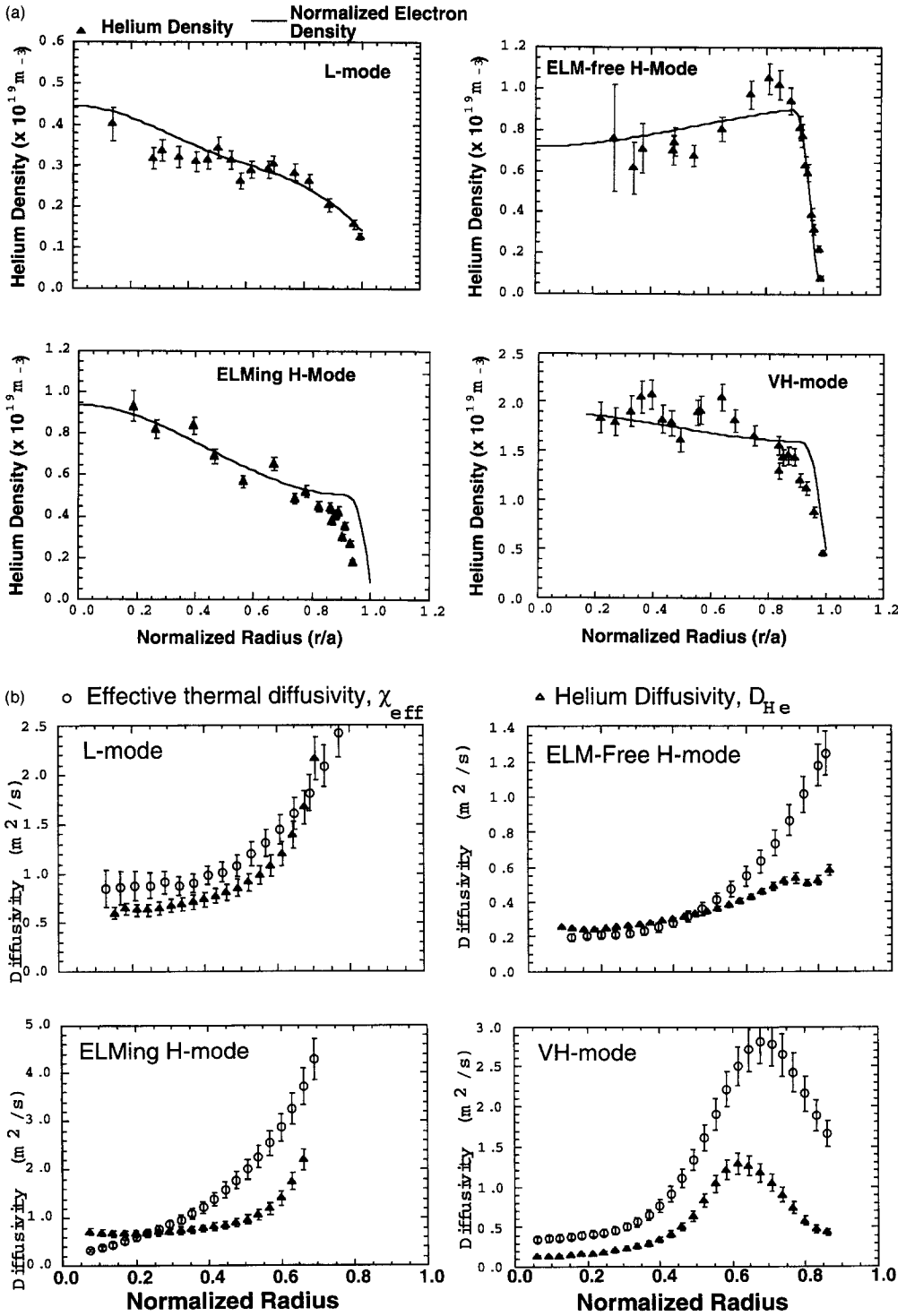

Fig. 5. L-mode, ELMy H-, ELM-free H- and VH-mode comparison for DIII-D, (a) n_e, n_{He} profiles, (b) D, χ profiles.

helium fueling efficiency for neutral beams relative to helium gas puffing. The helium gas puff strength was equivalent in number to that which would be produced by 0.6 GW of fusion power [78].

To date there is no indication of a difference in helium content between neutral injection and gas puffing cases in basic confinement and divertor regimes. Presumably this is so because edge recycling dominates the helium content, as it will in future long pulse reactors.

4.2. Divertor / edge transport: $\tau_{div}(\gamma, \varepsilon)$

Somewhat pessimistic trends showing that divertor helium enrichment decreases with increasing average n_e were reported in the earlier generation of helium divertor experiments in Doublet III and JT-60 (see Fig. 9 in Ref. [1]). A more favorable trend was observed with neutral beam injection [76]. However, because of the importance of demonstrating satisfactory values for the reactor criteria (ρ_{WR} and η) most study of divertor helium processes has occurred in integrated helium removal experiments (discussed in Section 4.3.3). The relatively few experiments carried out specifically to study helium edge and divertor processes have been done in the basic edge and divertor modes (limiter and high recycling divertor).

4.2.1. Limiter experiments

Fundamental helium exhaust data have been verified in a Tore Supra test of a novel vented limiter structure, as proposed in Ref. [79]. The design relies on Franck–Condon dissociation of the limiter-recycled D^+ flux to produce a significant D^0 pressure buildup for pumping in a plenum behind the vents. Because of the low cross sections for helium charge exchange processes, though, the helium pressure is found to be about 4 times lower than that found under similar conditions in the 'classical' outboard pump limiter [38]. This result is consistent with modeling by the JONAS code [80]. Helium particle control and pumping experiments using the Outboard Pump Limiter in Tore Supra showed that an accurate plasma density balance could be obtained for helium discharges in an all-graphite environment [81].

Similarly, processes in the ALT-II pump limiter throat have tested divertor modeling codes. Experiments have been carried out with the aim of understanding the observed tendencies in removal efficiency and their connection to modeling. The helium back-conductance from the pump limiter throat increases with the throat density and this trend is reproduced with coupled EIRENE neutral transport and core impurity radial transport calculations [82,83]. Using this technique one can deduce the helium removal efficiency (ε) separately from the overall exhaust efficiency (which depends on repenetration and back-conductance) (Mank in Ref. [41]).

4.2.2. Conventional high recycling divertor / ELMy H-mode

Scans of strike point position in unpumped DIII-D discharges show that there is significant dilution of helium from the core to the baffle region. The helium concentration is sensitive to the strike point location (indicating the peak of the D^+ particle flux) under ohmic conditions, but there is little sensitivity to this position with increased neutral beam injection. Divertor enrichment values $\eta \sim 0.4$ have been measured, deteriorating with increased neutral beam power [24]. Helium divertor experiments on DIII-D have been analyzed using an upgraded version of the b2 divertor transport code [84]. A database of divertor cases has been constructed, varying D, V, χ, R_{He}, and R_D. The observed power dependence of helium separation was reproduced with the hypothesis that the scrape-off layer diffusivity increases in the same way with an increase in power as does the core diffusivity [21].

Experiments are in progress on JT-60U to investigate the dependence of the asymmetry in helium peaking at the inner and outer strike points on core and edge conditions [85].

4.3. Integrated helium removal experiments: τ_{div}, $\tau_{pump}(\gamma, \varepsilon)$

Integrated helium transport and exhaust experiments have been carried out with basic edge and divertor conditions (limiter and high recycling divertor) combined with basic and enhanced core confinement modes (Section 4.3.1), and in enhanced divertor and edge perfomance modes: detached divertor, completely detached H-mode, and with a radiative edge decoupling the core from the limiter (Section 4.3.2). There is by now an appreciable database of integrated helium transport and exhaust experiments (Section 4.3.3).

4.3.1. Basic edge / divertor perfomance: Limiter, conventional high recycling

4.3.1.1. Gas puff source in ELMy H-mode. The first helium exhaust experiments in ELMy H-mode conditions were carried out on DIII-D, using the argon frost technique. The resulting values of ρ_{WR} were found to be adequate for reactor requirements [35]. Fig. 4 (also described in Section 4.1.2) shows the details of the pumping experiment. When the outer divertor strike point is moved to the baffle entrance the helium pressure builds up in the baffle, pumping begins, and the helium content begins to decay both in the baffle and in the core plasma. Helium baffle pressures are measured with a species-selective Penning gauge.

Helium exhaust experiments have been conducted in JET under both L- and H-mode conditions, both with and without argon frost on the divertor cryopump. In L-mode there is a constant helium content ($R_{He} \sim 1$) without argon

frost, and a steady decay in the core helium density with argon frost. However, in H-mode little decay in the helium content is observed in the case with argon frost. The global parameter $\rho_{WR} \sim 20$ for H-mode and $\rho_{WR} \sim 10$ for L-mode. Fig. 6 shows the comparison between L-mode and H-mode helium exhaust in JET. Further studies are underway to understand the relation between helium exhaust in H-mode and the details of the JET divertor and pumping geometry. The observed value of τ_α/τ_E for helium *core* transport is not limiting for future machines. However, argon frost pumping has also been found to be unsatisfactory for long pulse length discharges in JET, due to the deterioration in pumping speed which is caused by coverage of the argon frost layer with deuterium [29].

4.3.1.2. Central helium sources in high β_{pol} and ELMy H-mode. Helium exhaust was studied in JT-60U by using the intrinsic pumping from B_4C tiles on the divertor targets, by the process of solid target boronization (STB). In this way a constant helium core concentration was obtained with helium beam injection. Values of $\rho_{WR} = 6$–8 were obtained with STB, while $\rho_{WR} = 70$–100 resulted without STB. Fig. 7 shows helium beam injection and exhaust in high β_{pol} mode from JT-60U [78].

An integrated helium transport and exhaust experiment with both a central helium source (from helium beam injection) and an active pumping system (argon frost) has been carried out in DIII-D (Wade in Ref. [41]). This simulation showed-that centrally deposited helium could be efficiently exhausted with the cryo-pump system, with $\rho_{WR} \sim 8$. The helium profile became peaked with initiation of helium beam injection, but quickly relaxed to the pre-injection shape. ρ_{WR} was found to be insensitive to injected power for $\rho_{NB} = 4$–10 MW.

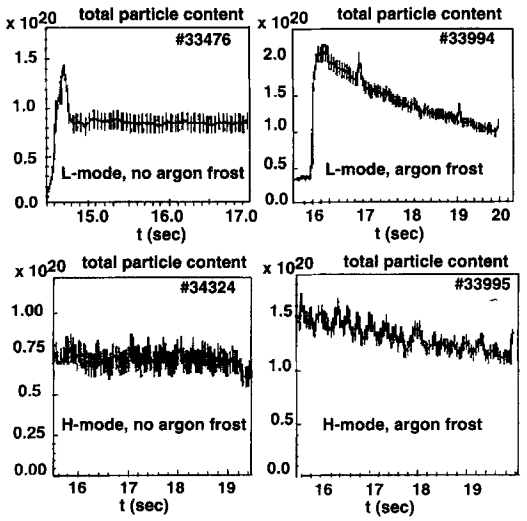

Fig. 6. JET helium exhaust in L-mode and H-mode conditions with and without argon frost pumping.

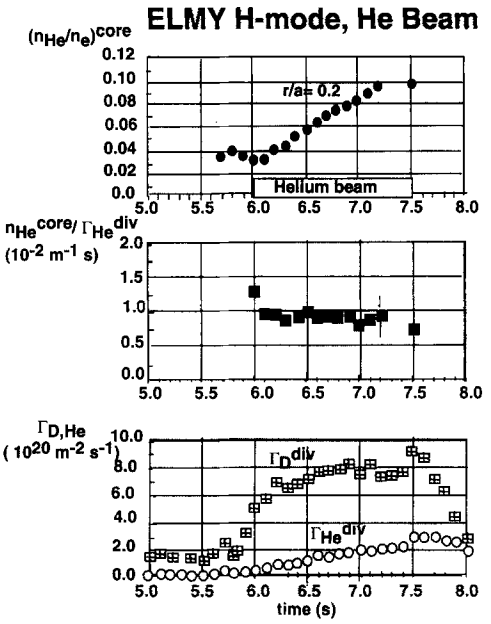

Fig. 7. Integrated helium transport and exhaust simulation experiment on JT-60U. Helium neutral beam injection, with exhaust by STB.

4.3.2. Enhanced divertor perfomance modes: Detached divertor, radiative edge

4.3.2.1. Detached divertor. Helium transport and exhaust experiments in detached plasma conditions on Tokamak des Varennes use a cryosorption exhaust technique. Experiments have been carried out in upper single null configurations. Detached plasmas have been obtained [39] at moderate densities ($n_e \sim 5 \times 10^{19}$ m^{-3}) and did diminish divertor pumping. Similar effects were observed with D_2 and helium retention. Exhaust was found to be adequate for D_2, but not for helium. A strong effect of divertor plate biasing in promoting helium exhaust was observed. Helium decay experiments examining the dependence with lower hybrid power showed enhanced confinement (decreased decay times τ_{He}) without additional power.

4.3.2.2. CDH mode. Helium exhaust has been found to be quite efficient under completely detached H-mode (CDH) conditions and an ITER-compatible helium divertor enrichment, $\eta = 0.3$, is attained. The CDH discharges are obtained with feedback-controlled neon puffing, and the radiated power is maintained stably at about 90% of the input power. Fig. 8 shows the helium decay in the core, inner wall, and divertor with $\rho_{WR} \sim 10$ (Bosch in these Proceedings) at the lower end of the neutral density range available in CDH mode. The helium decay rate, compression and enrichment factor all vary strongly with the neutral gas flux density in the divertor. If the divertor neutral density is increased, then there is faster helium decay with higher

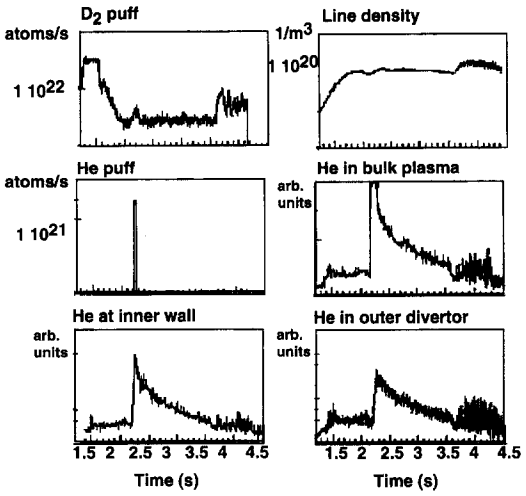

Fig. 8. Helium exhaust in completely detached H-mode (Asdex Upgrade) with $P_{rad}/P_{in} \sim 90\%$ achieved by feedback-controlled neon injection.

density and $\rho_{WR} \sim 7$ for neutral density at the highest neutral density available in CDH mode. The Divertor I configuration was used (see Table 1), with the ASDEX turbomechanical pump. The empirical time constants (τ_{plasma}, τ_{div}, τ_{pump}) are measured in these experiments, but cannot be directly compared to those needed in future machines, like ITER. Rather this must be investigated by modeling, which is thus an integral part of the ASDEX-Upgrade approach.

4.3.2.3. Radiative edge. Following earlier experiments in TEXTOR [40], experiments on TEXTOR-94 have been performed in which helium exhaust was conducted in highly radiating plasmas [86]. A good exhaust efficiency of helium was found in highly radiating cases. A density scan, with a radiated fraction up to 90%, showed that an increase in the ALT-II pump limiter exhaust efficiency partially compensated for the observed increase in the helium confinement time as the radiation fraction increased. In this case it is the removal efficiency which increases, because of increased friction between D- and He-ions. However, helium exhaust was not as efficient as neon exhaust in these experiments, and further work will be done.

4.3.3. Summary

Because of the wide variety of core plasma and divertor configurations and geometries, and the difference in exhaust methods, comparative experiments on several devices are needed to produce an extrapolable result for future machines. To date, this has been possible mostly for ELMy H-mode conditions in conventional high recycling divertor conditions. Encouraging results have been obtained both for enhanced core confinement regimes, and for enhanced divertor performance configurations, but as yet the database is restricted to isolated examples without much opportunity for cross-comparison. Nonetheless, there are now results from a number of integrated helium removal experiments. The (generally favorable) values for $\rho_{WR} = \tau_\alpha^*/\tau_E$ and for the divertor enrichment factor η are summarized in Table 2. Taken together, these results constitute a demonstration of the feasibility, under the proper conditions, of efficient helium removal from tokamaks. However, results for the relevant combination of enhanced core confinement, enhanced divertor performance and applicable divertor geometry have yet to be demonstrated.

5. Discussion

Although existing capabilities to study ITER-like core configurations and profiles for relatively short times are

Table 2
Results for typical global parameters for helium transport ($\rho_{WR} = \tau_\alpha{}^*/\tau_E$) and divertor enrichment, η

Global helium exhaust results				
tokamak	Pumping [a] type	ρ_{WR} ($\tau_\alpha{}^*/\tau_E$)	Divertor helium enrichment (η)	Confinement mode
Divertor				
JET MkI	Ar	10	–	L
		20	–	H
JT-60U	STB	6–8	0.4	high β_{pol}
	w/o STB	70–100		
DIII-D	Ar	8	0.500.6	ohmic
	–		0.4	ELMy H
Asdex-U	TM	7–10	0.3–0.5	CDH
TdeV	CS	10	0.15	L
Limiter				
TFTR	Wall	8–10	–	
TEXTOR	TM	8	–	

[a] Helium pumping: TM: turbomolecular, AR: argon frost, CS: cryosorption, STB: solid target boronization.

adequate, it is at present impossible to study ITER performance scenarios. Neither the divertor geometry nor the available pumping schemes at present can simulate the ITER requirements. In particular, study of the helium exhaust in the vertical target configuration has not been explored in experiments. Because of deficiencies in the argon frost technique, new helium pumping techniques are needed. For example the use of cryopumps combined with activated charcoal (Campbell in Ref. [41]) or the use of turbomechanical pumping (Loarer in Ref. [41]) is being explored.

Similarity constraints have been devised for core transport experiments to define operating conditions in which as many as possible of the relevant dimensionless parameters are the same as for future machines. However, this has not been done in the area of helium transport and exhaust. If it were, then helium processes could be examined under 'divertor similarity' conditions as close as possible to the relevant ones for future burning devices.

An earlier survey [87] gave the status of enhanced core and divertor modes which have been identified. Since that time new regimes have been studied for reversed shear and completely detached H-mode conditions. Neither helium core transport nor divertor and edge processes have been systematically examined in the improved regimes.

A core helium transport database is, however, coming into existence — results have been obtained for ohmic, L-, ELM-free H-, ELMy H-, and VH-modes as well as for supershot conditions. Work is presently in progress on TFTR and JT-60U to characterize helium transport in reverse shear modes. For divertor processes, in spite of inevitable limitations, modeling is the main tool to compare the effect of geometry on helium exhaust.

So there is a need both to carry out further detailed investigations of fundamental helium transport and exhaust processes in novel confinement and divertor regimes, and also to have the capability to simulate ITER-like performance scenarios in the geometry which is planned for this device. A rather wide spectrum of future experimental activity is thus indicated.

Acknowledgements

The authors wish to express their gratitude to the participants on the series of International Workshops on Helium Transport and Exhaust (Gatlinburg, 1991; Monterey, 1992 and Charleston, 1995) for allowing us to draw on their results and their wisdom in preparing this review.

References

[1] D. Reiter et al., Plasma Phys. Control. Fusion 33 (1991) 1579.
[2] D.J. Rose, Nucl. Fusion 9 (1969) 183.
[3] S. Saito, M. Sugihara, N. Fujisawa, K. Ueda and T. Abe, Nucl. Technol./Fusion 4 (1983) 498.
[4] D.F. Duechs and D. Pfirsch, IAEA, Vienna, Tokyo, Vol. 1 (1974) 669.
[5] M. Shimada, M. Nagami, K. Ioki et al., Phys. Rev. Lett. 47 (1981) 796.
[6] R.J. Fonck and R.A. Hulse, Phys. Rev. Lett. 52 (1984) 530.
[7] Y. Seki, Y. Shimomura, K. Maki, M. Azumi and T. Takizuka, Nucl. Fusion 20 (1980) 1213.
[8] K.-H. Finken, K.H. Dippel, W.Y. Baek and A. Hardtke, Rev. Sci. Instrum. 63 (1992) 1.
[9] D. Post and S. Cohen, ITER Physics Group, IAEA, ITER Physics (1990).
[10] J.T. Hogan and D. Hillis, Nucl. Fusion 31 (1991) 2181.
[11] J.T. Hogan and D. Hillis, Nucl. Fusion 32 (1992) 2055.
[12] J. Strachan and A. Chan, Nucl. Fusion 27 (1987) 1025.
[13] D.L. Hillis, J.T. Hogan, K.-H. Finken et al., Vol. 3 (IAEA, Vienna, Washington, DC, 1990) p. 587.
[14] D.L. Hillis, K.-H. Finken, J.T. Hogan et al., Phys. Rev. Lett. 65 (1990) 2382.
[15] H. Nakamura, K. Tobita, T. Hirayama et al., Fusion Technol. 18 (1990) 578.
[16] E.J. Synakowski, B. Stratton, P.C. Efthimion et al., Phys. Rev. Lett. 65 (1990) 2255.
[17] P.-H. Rebut et al., Phys. Fluids B3 (1991) 2209.
[18] D.L. Hillis, J. Hogan, K.-H. Finken et al., J. Nucl. Mater. 196-198 (1992) 35.
[19] D.L. Hillis et al., Wurzburg IAEA, Vol. CN-56 (IAEA, Vienna, Wurzburg, Germany, 1992) p. A-7-20.
[20] D.L. Hillis, M.R. Wade, J.T. Hogan et al., Plasma Phys. Control Fusion 36 (1994) A171.
[21] D.L. Hillis, M.R. Wade, J.T. Hogan et al., Vol. CN-60/A2 (IAEA, Sevilla, Spain, 1994) p. 4-P-11.
[22] M.R. Wade, D.L. Hillis, D.F. Finkenthal et al., 21st EPS, Vol. 17C (EPS, Lisboa, Portugal, 1993) p. 63.
[23] M.R. Wade, J.T. Hogan, D.L. Hillis et al., Fusion Technol. 26 (1994) 595.
[24] M.R. Wade, J. Hogan, D. Hillis et al., J. Nucl. Mater. 220–222 (1994) 178.
[25] E.J. Synakowski, R. Bell, R. Budny et al., Phys. Rev. Lett. 75 (1995) 3689.
[26] E.J. Synakowski, P.C. Efthimion, G. Rewoldt et al., Phys. Fluids B5 (1993) 2215.
[27] E.J. Synakowski, P.C. Efthimion, G. Rewoldt et al., Vol. CN-56 (IAEA, Vienna, Wuerzburg, Germany, 1992) p. A-7-16.
[28] P.C. Efthimion, L.C. Johnson, C.H. Skinner et al., Vol. CN-60 (IAEA, Vienna, Sevilla, Spain, 1994) p. A-2-II-6.
[29] M.G. v. Hellermann, K. Barth, A. Bickley et al., 22nd Eur. Conf. Contr. Fusion Plasma Phys., Vol. 19C, Part II (EPS, Bournemouth, UK, 1995) p. 11-009-012.
[30] M.G. v. Hellermann, W.G.F. Core, J. Frieling et al., Plasma Phys. Control Fusion 35 (1993) 799.
[31] L.D. Horton, B. Denne-Hinnov, A. Gondhalekar et al., Vol. CN-56 (IAEA, Vienna, Wuerzburg, Germany, 1992) p. A-7-4.
[32] T. Sugie, K. Itami, H. Nakamura et al., Vol. CN-53 (IAEA, Vienna, Washington, DC, US, 1990) p. A-5-4.
[33] A. Sakasai, Y. Koide, H. Nakamura et al., JT60 EPS, 21st EPS, Vol. 17C (EPS, Lisbon, Portugal, 1993) p. 67.
[34] A. Sakasai, H. Kubo, N. Hosogane et al., IAEA, Vienna, Seville, Spain (1994).

[35] M.R. Wade, D.L. Hillis, J.T. Hogan et al., Phys. Rev. Lett. 74 (1995) 2702.
[36] K. Lackner, H.-S. Bosch, D. Coster et al., Plasma Phys. Control Fusion 36 (1994) B79.
[37] G. Haas, H.-S. Bosch, A. Kallenbach et al., Proc. 22th EPS Conf. Contr. Fusion Plasma Phys., Vol. 19C, Part I (Bournemouth, UK, 1995) p. 321.
[38] T. Loarer, M. Chatelier, A. Grosman et al., Plasma Phys. Control Fusion 37 (1995) A203.
[39] R. DeCoste, J.-L. Gavreau, G. Abel et al., 3rd IAE Workshop on Helium Transport and Exhaust in Tokamaks (Charleston, 1995).
[40] U. Samm, J. Boedo, G. Bertschinger et al., J. Nucl. Mater. 196–198 (1992) 633.
[41] J.T. Hogan and D. Hillis, Nucl. Fusion (1996) in press.
[42] D. Reiter, G. H. Wolf and H. Kever, Nucl. Fusion 30 (1990) 2141.
[43] G. Janeschitz, G. Fussmann and P.B. Kotze et al., Nucl. Fusion 26 (1986).
[44] J. Neuhauser, R. Aratari, M. Bessenrodt-Weberpals et al. (IAEA Vienna, Washington, DC, 1990), Vol. IAEA-CN-53/A-5-52.
[45] U. Samm, M. Z. Tokar' and B. Unterberg, 22nd EPS, Vol. 19C, Part II (EPS, Bournemouth, UK, 1995) p. 11–201-204.
[46] N. Noda, in: Contributions to High-Temperature Plasma Physics, eds. K.A. Spatschek and J. Uhlenbusch (Akademie Verlag, Berlin, 1994) p. 21.
[47] G. Janeschitz, K. Borrass, G. Federici et al., J. Nucl. Mater. 220–222 (1994) 73.
[48] G. Janeschitz, ITER JCT, ITER Home Teams, Plasma Phys. Control Fusion 37 (1995) A19.
[49] G. Janeschitz and K. Borrass, Nucl. Fusion 35 (1995) 1203.
[50] R.A. Hulse, Nucl. Technol./Fusion 3 (1983) 259.
[51] H.P. Summers and W.J. Dickson, in: Recombination of Atomic Ions, ed. W.G. Graham (Plenum, New York, 1992).
[52] B.J. Braams, thesis, A multi-fluid code for simulation of the edge plasma in tokamaks (1987).
[53] P.C. Stangeby, Nucl. Fusion 28 (1988) 1945.
[54] P.C. Stangeby and J.D. Elder, J. Nucl. Mater. 196–198 (1992) 258.
[55] K. Itoh, N. Ueda, S.-I. Itoh et al., Simulation on the Ash Exhaust in Fusion Engineering Device, Hiroshima Univ., Inst. for Fusion Theory (1988).
[56] S.I. Krasheninnikov, Contrib. Plasma Phys. 28 (1988) 465.
[57] S.I. Krasheninnikov, A.S. Kukushkin and T.K. Soboleva, Nucl. Fusion 31 (1991) 1455.
[58] S.A. Cohen, K.A. Werley, D.E. Post et al., J. Nucl. Mater. 176&177 (1990) 909.
[59] D. Reiter, J. Nucl. Mater. 196–198 (1992) 80.
[60] R. Schneider, D.P. Coster, J. Neuhauser et al., 22nd EPS, Vol. 19C, Part IV (EPS, Bournemouth, UK, 1995) p. IV-285.
[61] G. Maddison and M. Baelmans, 22nd EPS, Vol. IV (EPS, Bournemouth, UK, 1995) p. IV-309.
[62] R. Schneider et al., J. Nucl. Mater. 220–222 (1995) 1076.
[63] A. Kukushkin et al., 22nd EPS, Vol. IV (EPS, Bournemouth, UK, 1995) p. IV-329.
[64] P. Bachmann, D. Reiter and A. Prinja, J. Nucl. Mater. 220–222 (1992) 856.
[65] P. Bachmann and D. Reiter, Contrib. Plasma Phys. 35 (1995) 45.
[66] B.Q. Deng, Z.Y. Xie, H.W. Shi et al., Contrib. Plasma Phys. 33 (1993) 35.
[67] G.S. Saibene et al., 21st EPS (EPS, 1992).
[68] A.T. Ramsey and D.M. Manos, J. Nucl. Mater. 196–198 (1992) 509.
[69] M.M. Menon, P.M. Anderson, C.B. Baxi et al., Fusion Technol. 22 (1992) 356.
[70] H.-S. Bosch, D., 3rd IAE Workshop on Helium Transport and Exhaust (Charleston, 1995).
[71] H.-S. Bosch, R. Dux, G. Haas et al., Phys. Rev. Lett. 76 (1996) 2499.
[72] D. Sigmar, C.Z. Cheng, G.J. Sadler and S.J. Zweben, Nucl. Fusion 35 (1996) 1421.
[73] G. McKee et al., Phys. Rev. Lett. 75 (1995) 649.
[74] R. Goldston, J. Comput. Phys. 43 (1981) 161.
[75] D. Finkenthal, D. Hillis, M. Wade et al. (EPS, Innsbruck, Austria, 1992).
[76] H. Nakamura, T. Hirayama, Y. Koide et al., Phys. Rev. Lett. 67 (1991) 2658.
[77] K. Tobita, T. Itoh, A. Sakasai et al., Plasma Phys. Control Fusion 32 (1990) 429.
[78] A. Sakasai, H. Kubo, N. Hosogane et al., J. Nucl. Mater. 220–222 (1994) 405.
[79] H.H. Abou-Gabal and G.A. Emmert, Nucl. Fusion 31 (1991) 407.
[80] E. Tsitrone, thesis, Université de Provence, Marseilles (1996).
[81] T. Uckan et al., 22nd EPS (EPS, Bournemouth, UK, 1995).
[82] D. Reiter, Forschungszentrum, Juelich, The Eirene Code, Version: Jan. 92, Users' Manual (1992).
[83] M. Baelmans et al., 22nd EPS, Vol. IV (EPS, Bournemouth, UK, 1995) p. IV-321.
[84] R. Maingi, J. Hogan, P. Mioduszewski et al., Nucl. Fusion 34 (1994) 283.
[85] A. Sakasai, private communication (1996).
[86] G. Mank, U. Samm, K.H. Finken et al., 22nd EPS, Vol. 19C, Part II (EPS, Bournemouth, UK, 1995) p. 1-057.
[87] S.-I. Itoh, K. Itoh and A. Fukuyama, J. Nucl. Mater. 220–222 (1995) 117.